Physics and Imaging in Radiation Oncology 16 (2020) 130–133

Contents lists available at ScienceDirect

Physics and Imaging in Radiation Oncology

journal homepage: www.sciencedirect.com/journal/physics-and-imaging-in-radiation-oncology

Technical Note

Imaging performance of a high-field in-line magnetic resonance imaging linear accelerator with a patient rotation system for fixed-gantry radiotherapy

Jarryd G. Buckley [a,b,*], Bin Dong [b,c], Gary P. Liney [b,c]

[a] Centre for Medical Radiation Physics, University of Wollongong, Northfields Avenue, Wollongong, NSW 2522, Australia
[b] Ingham Institute for Applied Medical Research, 1 Campbell St, Liverpool, NSW 2170, Australia
[c] Liverpool and Macarthur Cancer Therapy Centre, Liverpool Hospital, 75 Elizabeth St, Liverpool, NSW 2170, Australia

ARTICLE INFO

Keywords:
MRI-Linac
Patient rotation
Radiation therapy

ABSTRACT

This paper describes the imaging performance of a high-field in-line MRI linear accelerator with a patient rotation system in-situ. Signal quality was quantified using signal-to-noise ratio (SNR) and RF uniformity maps. B0-field inhomogeneity was assessed using magnetic field mapping. SNR was evaluated with various entries into the Faraday cage which were required for extended couch translations. SNR varied between 103 and 87 across PRS rotation angles. Maximum B0-field inhomogeneity corresponded to 0.7 mm of geometric distortion. A 45 × 55 cm^2 aperture allowed PRS translation with no reduction in SNR. Imaging performance with the PRS in-situ was found to be acceptable.

1. Introduction

External beam radiotherapy requires relative rotation between the patient and x-ray beam to intersect a tumour from multiple angles to maximise tumour dose whilst minimising the dose to surrounding tissue. Rotation is usually achieved by rotating the x-ray source on a gantry with the patient lying on a treatment table. An alternative approach would be to instead rotate the patient using a patient rotation system (PRS) – removing the gantry would make radiotherapy systems cheaper, opening up the potential to increase access to radiotherapy globally [1,2]. While commercial MRI-Linac systems currently use a rotating x-ray beam oriented perpendicular to the main magnetic field [3,4], MRI-guided radiotherapy is particularly suited to patient rotation because of its exquisite soft-tissue contrast, which is necessary to visualise anatomical motion during rotation [5]. A fixed radiation source also avoids potential B0-field inhomogeneity which is associated with the rotating gantries [6]. During the installation and commissioning of commercial MRI-Linac systems, these inhomogeneities must be characterised and appropriately shimmed [7].

Incorporating a PRS with an MRI-linac necessitates additional materials be placed within the MRI which may attenuate the RF signal, introduce RF noise and degrade the B0-field homogeneity [8,9]. In the context of MRI-guided radiotherapy, image quality must remain adequate for accurate delineation of the tumour from surrounding healthy tissue and maintain sum-millimetre geometric precision [10]. Therefore, any degradation in image quality due to the presence of a PRS within the MRI-linac must be quantified and understood.

This paper describes testing of the image performance of a PRS currently under development for a high-field in-line MRI-Linac.

2. Materials and methods

2.1. Patient rotation system design

The patient bed lift and rotate mechanics and the tray in which all the components are housed were constructed from fibreglass to minimise geometric distortion and attenuation of the RF signal. The PRS was supported by an aluminium structure which translated into the MRI under the transmit/receive body coil. Two stainless steel driveshafts, which supply mechanical power to the lift/rotate mechanism on the far end of the PRS remained within the body coil, but approximately 30 cm below the imaging isocentre. The materials used for construction of the PRS were chosen based on initial pilot imaging tests. Prior to imaging tests, safety tests were carried out with the device in situ, with no magnetic forces apparent. RF heating tests were previously performed with our system as a whole, with negligible heating observed [11]. It

* Corresponding author.
E-mail address: jgb552@uowmail.edu.au (J.G. Buckley).

https://doi.org/10.1016/j.phro.2020.11.001
Received 10 June 2020; Received in revised form 5 November 2020; Accepted 5 November 2020
Available online 18 November 2020

was not expected that the presence of the PRS would affect RF heating given the field strength of 1 T and non-conductive materials used in the PRS design. The potential introduction of eddy currents was checked by performing an eddy current compensation tune-up with the PRS in the scanner. All results were within system specifications.

2.2. Imaging performance during PRS rotation

Signal quality was assessed using signal-to-noise ratio (SNR) and RF uniformity maps. Both the SNR and RF uniformity maps were evaluated with a 24 cm diameter spherical body phantom for PRS rotation angles of 0, 90, and 180-degrees. Images were acquired at each PRS rotation angle using an agreed clinical protocol T1 spin-echo sequence (TR: 1000 ms, TE: 30 ms, slice thickness: 5 mm, Field of View: 300 × 300 mm^2 scan time: 4:20). The phantom was doped with 1.25 g of $NiS0_4 \times 6H_20$ per 1000 g of distilled H_20 to simulate the RF signal produced by human tissue. SNR was calculated by dividing the mean signal within a spherical ROI in the centre of the image ($S_{ROI\ 1}$) by the standard deviation of a background ROI outside the phantom (S-$D_{ROI\ 2}$) [12]:

$$SNR = \frac{S_{ROI1}}{S - D_{ROI2}} \quad (1)$$

RF uniformity maps, which are affected by RF transmission and reception, were calculated by comparing the mean signal within a circular region-of-interest (ROI) in the centre of the body phantom to pixel intensities within the entire phantom (in the axial plane) [9]. The ROI had a surface area equal to 10% of the total phantom area.

Potential distortion from non-uniformity in the B0-field at each PRS rotation angle was assessed using a duel-echo gradient field mapping sequence with TE's of 10 ms and 17.22 ms. B0-field maps were chosen over phantom based distortion measurements as they provided a more accurate distortion measurement which can be applied to any sequence. The sequence generated magnitude and phase images were used to create B0-field maps using the open source software SPM, which included phase unwrapping prior to calculation of each B0-field map (The Wellcome Centre for Human Neuroimaging, UCL Queen Square Institute of Neurology, London, UK). The maximum distortions measured in frequency Δf were calculated from the maximum point-to-point phase differences Δϕ in each B0-field map using equation (2):

$$\Delta f(\mathrm{Hz}) = \frac{\Delta\phi}{2\pi\Delta TE} \quad (2)$$

T2-weighted turbo spin-echo images were also acquired of an MRI-compatible head phantom at each PRS rotation angle to qualitatively verify that anatomical image quality was consistent for each PRS rotation angle (TR: 10260 ms, TE: 86 ms, slice thickness: 5 mm, Field of View: 384 × 308 mm^2 scan time: 6:40).

2.3. Imaging performance with varying faraday cage apertures

To allow imaging of any anatomical position it was necessary to translate the PRS such that the middle of the PRS bed reached the MR imaging isocentre. For extended translation, an aperture in the far end of the Faraday cage was required. Three tests were trialled: Faraday cage closed to obtain baseline image quality, a 48 × 55 cm^2 aperture, which was the minimum size to allow translation of the PRS through the cage, and completely removing the 130 × 167 cm^2 side panel as a worst case. For each configuration, SNR was evaluated with the PRS in the 0-degree position. SNR values were compared with the linear accelerator and multi-leaf collimators (MLC's) turned off, then on, to investigate any introduction of RF interference from this source.

3. Results

SNR values of 103, 95 and 87 were measured for PRS rotation angles 0, 90 and 180 degrees, respectively. B0-field maps for each PRS rotation angle are shown in Fig. 1. Maximum peak-to-peak variations in frequency were 76 Hz (1.52 ppm), 83 Hz (1.95 ppm) and 79 Hz (1.64 ppm), respectively. For the imaging bandwidth of 260 Hz per pixel, this corresponded to ≈ 0.3 pixels of distortion or 0.7 mm for the pixel width of 2.3 mm. The largest distortions were observed at the base of the phantom.

RF uniformity maps for each PRS rotation angle are shown in Fig. 1. The RF signal was within 20% of the centre ROI within the central 20 cm of the spherical body phantom and decreased beyond 20% toward the phantom periphery for each PRS couch angle.

Anatomical images of the head phantom for each PRS rotation angles are shown in Fig. 2. Anatomical image quality was consistent at each PRS rotation angle with no geometric distortion or signal variation present.

With the Faraday cage closed, SNR was measured to be 32 and 31 with the x-ray source and MLCs off and on, respectively. SNR with a 48x 55 cm^2 aperture was 29 with the x-ray source and MLCs on. A test with the x-ray source and MLCs off was unnecessary since the SNR was consistent with the closed cage results which did not increase when the x-ray source and MLCs were turned off. With the side panel removed and the x-ray source and MLC's off, the SNR dropped to 6. A test with the x-ray source and MLCs on was not performed since SNR without the x-ray source or MLCs on was already too low for the panel removed to be a workable solution.

4. Discussion

In this paper we have described our initial findings with respect to image quality using a prototype patient rotation system for a high-field in-line MRI-Linac. With the PRS in-situ, geometric distortion was within 1.6 ppm, which could likely be accounted for with active shimming, and is consistent with commercial MRI-Linac systems for a DSV of 20 cm [13,14]. A previous study by Shan *et al.* quantified the B0-field inhomogeneity of the MRI-Linac used in this study, using the same B0 mapping approach [15]. They measured the inhomogeneity to be 80 Hz which corresponded to geometric distortions of 0.71 mm. Therefore, the presence of the PRS did not introduce B0-field inhomogeneity beyond what already exists with the system. Rotation of the PRS caused a small increase in distortion on the inferior region of the imaging volume, which was attributed to the presence of stainless-steel drive shafts within the PRS bed. A subsequent test showed that increasing the vertical height of the PRS bed by 4 cm, such that the phantom was further from the drive shafts, removed most of the signal non-uniformity from the image. During the design of the MRI-Linac used in this study, a small reduction in image quality was accepted to allow for a 50 cm gap between the magnets. This design provides a more open experience for the patient compared with the closed bore commercial MRI-Linac designs [16]. Additionally, the commercial MRI-linac systems are equipped with receiver coils with an associated increase in SNR. The MRI-Linac used in this study currently uses a uniform transmit/receive coil for all imaging.

Variation of the PRS rotation angle resulted in a small change in RF uniformity, which was also attributed to the stainless-steel drive shafts. Increasing the vertical height of the PRS couch so the imaging volume was further from the drive shafts improved RF uniformity. Spin-echo sequences, which will be used to verify a patients' set-up position prior to treatment, are unlikely to be impacted by the magnitude of distortion or RF uniformity loss, as was verified by the head phantom imaging. However, for steady state gradient-based sequences, which will be necessary for real-time imaging during x-ray treatment delivery, this reduction in image quality will have to be considered.

A 48 × 55 cm^2 aperture in the Faraday cage allowed the necessary PRS translation without compromising SNR, including during x-ray beam delivery. Another approach which was not considered, would be to modify the side panel to include a recess which would allow the necessary couch translation without the requirement of an aperture in the Faraday cage. However, based on the results presented, this will not

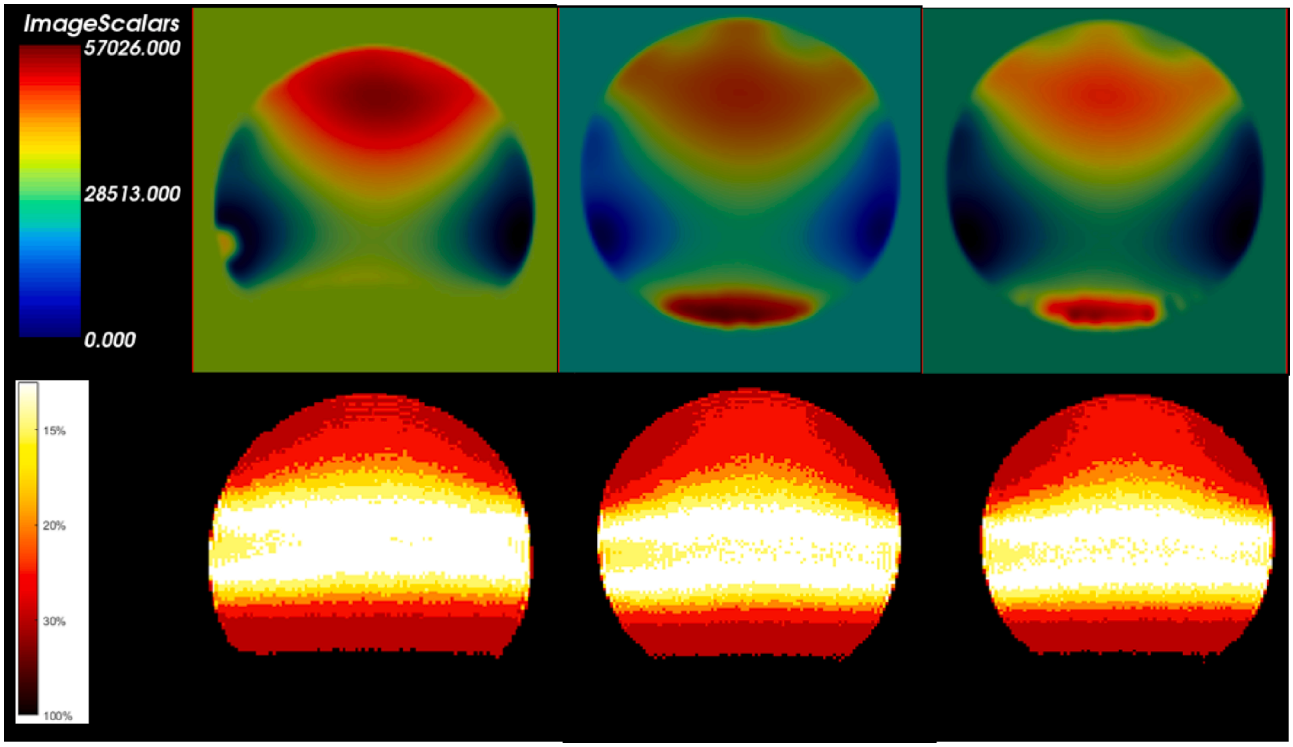

Fig. 1. Top row: B0-field maps at the 0, 90 and 180-degree PRS rotation angles. B0-field maps were acquired in the coronal plane through the centre of the spherical body phantom which was positioned at the MR imaging isocentre. The image pixel values ranged from 0 to 65,535 which corresponds to a phase change $\Delta\phi$ of $\pm\pi$, respectively. Bottom row: RF uniformity maps for PRS rotation angles of 0, 90 and 180-degrees. The colour scale indicates % change in signal intensity relative to a ROI in the centre of the phantom.

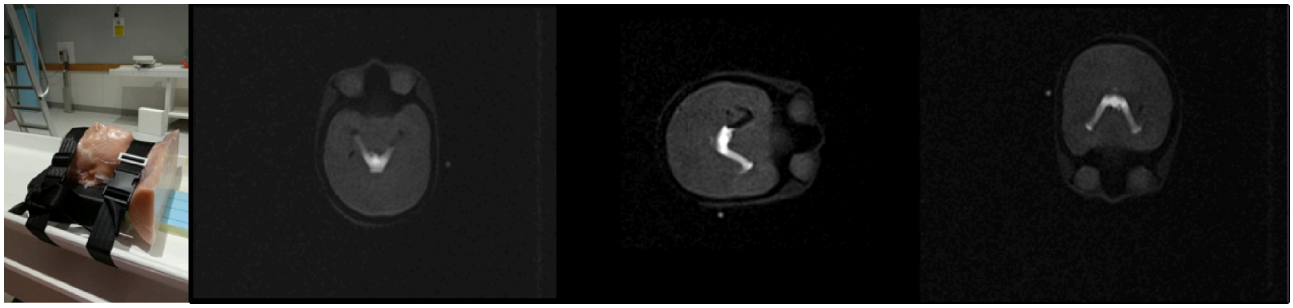

Fig. 2. Bottom row: Head phantom images at 0, 90 and 180-degree PRS rotation angles.

be necessary. Further, a receiver coil is currently in development which will be positioned over the PRS close to the patient surface. Since the receiver coil will greatly increase SNR, it is reasonable to conclude that any small increase in noise caused by the 48 × 55 cm^2 aperture will be acceptable.

The variation in SNR observed in this study is small compared with what has been observed with other MRI-Linac systems which require the radiation beam to traverse the RF receiver coil for some beam placements [17]. The SNR drop due to radiation induced currents in the coils for these systems must be mitigated through the application of build-up material to the coils [18] or by applying post-processing to the raw image data [17]. This is not an issue for the MRI-Linac used in our study as the transmit/receive coil is radiotransparent with no impact on either the imaging or dosimetry performance with a simultaneous radiation beam [11].

This imaging performance study only considered SNR, B0-field inhomogeneity and RF uniformity in one imaging plane. Additionally, the tests were performed with the PRS at a fixed vertical height (to position the phantom at imaging isocentre). Once the system is complete, a full characterisation of the imaging performance of the system will be undertaken including balanced gradient imaging for real-time motion management during radiation delivery.

A prototype patient rotation system for a high-field in-line MRI-Linac has been developed. MR-image quality was maintained for PRS rotation angles of 0, 90 and 180-degrees, and with an aperture in the Faraday cage sufficient to allow the required PRS translation. A small amount of image distortion was present on the B0-field maps and a lower vertical limit may therefore need to be set for balanced gradient-based sequences which will be used for real-time imaging during x-ray treatment delivery.

Funding

This work was supported by an NHMRC program grant (APP1132471).

Declaration of Competing Interest

The authors declare that they have no known competing financial interests or personal relationships that could have appeared to influence

the work reported in this paper.

Acknowledgements

This paper is part of a special issue that contains contributions originally submitted to the scientific meeting MR in RT, which was planned to take place 05/2020, organized by the German Research Center (DKFZ) in Heidelberg. We acknowledge funding by DKFZ for the publication costs of this special issue.

References

[1] Eslick EM, Keall PJ. The nano-X linear accelerator: a compact and economical cancer radiotherapy system incorporating patient rotation. Technol Cancer Res Treat 2015;14:565–72. https://doi.org/10.7785/tcrt.2012.500436.
[2] Whelan B, Welgampola M, McGarvie L, Makhija K, Turner R, Holloway L, et al. Patient reported outcomes of slow, single arc rotation: do we need rotating gantries? J Med Imaging Radiat Oncol 2017;62:553–61. https://doi.org/10.1111/1754-9485.12688.
[3] Winkel D, Bol GH, Kroon PS, van Asselen B, Hackett S, Werensteij-Honingh A, et al. Adaptive radiotherapy: the Elekta Unity MR-linac concept. Clin Transl Radiat Oncol 2019;18:54–9. https://doi.org/10.1016/j.ctro.2019.04.001.
[4] Mutic S, Dempsey JF. The ViewRay system: magnetic resonance-guided and controlled radiotherapy. Semin Radiat Oncol 2014;24:196–9. https://doi.org/10.1016/j.semradonc.2014.02.008.
[5] Buckley J, Rai R, Liney G, Dowling J, Holloway L, Metcalfe P, et al. Anatomical deformation due to horizontal rotation: towards gantry-free radiation therapy. Phys Med Biol 2019;64:175014. https://doi.org/10.1088/1361-6560/ab324c.
[6] Raaymakers B, Lagendijk J, Overweg J, Kok J, Raaijmakers A, Kerkof E, et al. Integrating a 1.5 T MRI scanner with a 6 MV accelerator: proof of concept. Phys Med Biol 2009;54:N229. https://doi.org/10.1088/0031-9155/54/12/N01.
[7] Tijssen RH, Philippens ME, Paulson ES, Glitzner M, Chugh B, Wetscherek A, et al. MRI commissioning of 1.5 T MR-linac systems–a multi-institutional study. Radiother Oncol 2019;132:114–20. https://doi.org/10.1016/j.radonc.2018.12.011.
[8] Xing A, Holloway L, Arumugam S, Walker A, Rai R, Juresic E, et al. Commissioning and quality control of a dedicated wide bore 3T MRI simulator for radiotherapy planning. Int J Cancer Ther Oncol 2016;4:1–10. https://doi.org/10.14319/IJCTO.42.1.
[9] Liney G, Owen S, Beaumont A, Lazar V, Manton D, Beavis A. Commissioning of a new wide-bore MRI scanner for radiotherapy planning of head and neck cancer. Br J Radiol 2013;86:20130150. https://doi.org/10.1259/bjr.20130150.
[10] Walker A, Liney G, Metcalfe P, Holloway L. MRI distortion: considerations for MRI based radiotherapy treatment planning. Australas Phys Eng Sci Med 2014;37:103–13. https://doi.org/10.1007/s13246-014-0252-2.
[11] Liney GP, Dong B, Weber E, Rai R, Destruel A, Garcia-Alvarez R, et al. Imaging performance of a dedicated radiation transparent RF coil on a 1.0 Tesla inline MRI-linac. Phys Med Biol 2018;63:135005. https://doi.org/10.1088/1361-6560/aac813.
[12] Firbank M, Coulthard A, Harrison R, Williams E. A comparison of two methods for measuring the signal to noise ratio on MR images. Phys Med Biol 1999;44:N261–4. https://doi.org/10.1088/0031-9155/44/12/403.
[13] Snyder JE, St-Aubin J, Yaddanapudi S, Boczkowski A, Dunkerley D, Graves S, et al. Commissioning of a 1.5 T Elekta Unity MR-linac: a single institution experience. J Appl Clin Med Phys 2020;21:160–72. https://doi.org/10.1002/acm2.12902.
[14] Ginn JS, Agazaryan N, Cao M, Baharom U, Low D, Yang Y, et al. Characterization of spatial distortion in a 0.35 T MRI-guided radiotherapy system. Phys Med Biol 2017;62:4525–40. https://doi.org/10.1088/1361-6560/aa6e1a.
[15] Shan S, Liney G, Tang F, Li F, Wang Y, Ma H, et al. Geometric distortion characterization and correction for the 1.0 T Australian MRI-Linac system using an inverse electromagnetic method. Med Phys 2020;47:1126–38. https://doi.org/10.1002/mp.13979.
[16] Liney GP, Whelan B, Oborn B, Barton M, Keall P. MRI-linear accelerator radiotherapy systems. Clin Oncol (R Coll Radiol) 2018;30:686–91. https://doi.org/10.1016/j.clon.2018.08.003.
[17] Burke B, Wachowicz K, Fallone B, Rathee S. Effect of radiation induced current on the quality of MR images in an integrated linac-MR system. Med Phys 2012;39:6139–47. https://doi.org/10.1118/1.4752422.
[18] Burke B, Ghila A, Fallone B, Rathee S. Radiation induced current in the RF coils of integrated linac-MR systems: The effect of buildup and magnetic field. Med Phys 2012;39:5004–14. https://doi.org/10.1118/1.4737097.